DOI: 10.1002/chem.200500365

Encapsulation of Cyanometalates by a Tris-macrocyclic Ligand Tricopper(II) Complex: Syntheses, Structural Variation, and Magnetic Exchange Coupling Pathways

Mihail Atanasov,[a, b] Peter Comba,*[a] Yaroslaw D. Lampeka,[a, c] Gerald Linti,[a] Thomas Malcherek,[d] Ronald Miletich,[d] Alexander I. Prikhod'ko,[a] and Hans Pritzkow[a]

Abstract: The reaction of $[M(CN)_6]^{3-}$ ($M = Cr^{3+}$, Mn^{3+}, Fe^{3+}, Co^{3+}) and $[M(CN)_8]^{4-/3-}$ ($M = Mo^{4+/5+}$, $W^{4+/5+}$) with the trinuclear copper(II) complex of 1,3,5-triazine-2,4,6-triyltris[3-(1,3,5,8,12-pentaazacyclotetradecane)] ($[Cu_3(L)]^{6+}$) leads to partially encapsulated cyanometalates. With hexacyanometalate(III) complexes, $[Cu_3(L)]^{6+}$ forms the isostructural host–guest complexes $[\{[Cu_3(L)(OH_2)_2]\text{-}[M(CN)_6]_2\}\{M(CN)_6\}]\cdot[M(CN)_6]\cdot 30\,H_2O$ with one bridging, two partially encapsulated, and one isolated $[M(CN)_6]^{3-}$ unit. The octacyanometalates of $Mo^{4+/5+}$ and $W^{4+/5+}$ are encapsulated by two tris-macrocyclic host units. Due to the stability of the +IV oxidation state of Mo and W, only assemblies with $[M(CN)_8]^{4-}$ were obtained. The Mo^{4+} and W^{4+} complexes were crystallized in two different structural forms: $[\{Cu_3(L)(OH_2)\}_2\{Mo(CN)_8\}]\text{-}(NO_3)_8\cdot 15\,H_2O$ with a structural motif that involves isolated spherical $[\{Cu_3(L)(OH_2)\}_2\{M(CN)_8\}]^{8+}$ ions and a "string-of-pearls" type of structure $[\{[Cu_3(L)]_2[M(CN)_8]\}\{M(CN)_8\}](NO_3)_4\cdot 20\,H_2O$, with $[M(CN)_8]^{4-}$ ions that bridge the encapsulated octacyanometalates in a two-dimensional network. The magnetic exchange coupling between the various paramagnetic centers is characterized by temperature-dependent magnetic susceptibility and field-dependent magnetization data. Exchange between the Cu···Cu pairs in the $[Cu_3(L)]^{6+}$ "ligand" is weakly antiferromagnetic. Ferromagnetic interactions are observed in the cyanometalate assemblies with Cr^{3+}, exchange coupling of Mn^{3+} and Fe^{3+} is very small, and the octacoordinate Mo^{4+} and W^{4+} systems have a closed-shell ground state.

Keywords: copper · host–guest systems · macrocyclic ligands · magnetic properties · self-assembly

Introduction

The ability of μ-bridging cyanide ions to lead to efficient pathways for metal···metal interactions has made cyanometalates useful and versatile building blocks for the design of new molecular magnetic materials.[1–6] After the first report of room-temperature magnets, obtained by the reaction of classical transition–metal hexacyanometalates $[M^a(CN)_6]^{m-}$ with aqua ions $[M^b(H_2O)_x]^{n+}$ (M^a,M^b = +II or +III transition–metal ion),[7] studies in this field were extended to other cyanometalates,[8–11] (for example, the photomagnetically active $[Mo(CN)_8]^{3-/4-}$ and $[W(CN)_8]^{3-/4-}$ complexes,[12,13] and $[Mo(CN)_7]^{4-}$ with an especially large magnetic anisotropy[14,15]) and to a variety of complexes of the type $[M^b(L)_y(solvent)_z]^{k+}$, which are able to encapsulate the cyanometalates to lead to discrete oligonuclear complexes.[15]

If L in a $[M^b(L)_y(solvent)_z]^{k+}$ complex blocks all but one of the positions in the coordination sphere of the metal ion

[a] Prof. Dr. M. Atanasov, Prof. Dr. P. Comba, Prof. Dr. Y. D. Lampeka, Prof. Dr. G. Linti, Dr. A. I. Prikhod'ko, Dr. H. Pritzkow
Universität Heidelberg, Anorganisch-Chemisches Institut
Im Neuenheimer Feld 270, 69120 Heidelberg (Germany)
Fax: (+49) 6221-546617
E-mail: peter.comba@aci.uni-heidelberg.de

[b] Prof. Dr. M. Atanasov
Institute of General and Inorganic Chemistry
Bulgarian Academy of Sciences, 1113 Sofia
"Acad. Georgi Bonchev" str. Bld.11 (Bulgaria)

[c] Prof. Dr. Y. D. Lampeka
L. V. Pisarzhevsky Institute of Physical Chemistry
National Academy of Science of Ukraine
Prospekt Nauki 31, 03039 Kiev-39 (Ukraine)

[d] Dr. T. Malcherek, Prof. Dr. R. Miletich
Universität Heidelberg, Mineralogisches Institut
Im Neuenheimer Feld 236, 69120 Heidelberg (Germany)

Supporting information for this article is available on the WWW under http://www.chemeurj.org/ or from the author.

M^b, the formation of isolated heterodinuclear complexes is possible. With pentaazamacrocyclic ligands L, very stable dinuclear complexes $[(L)Co^{III}CNFe^{II}(CN)_5]^-$ with interesting photochemical behavior were obtained.[16] With a variety of complexes of Cu^{2+}, Ni^{2+}, and Mn^{2+} the nuclearity of cyanometalate host–guest assemblies depends on the nature of the ligand L as well as on the anions present in the reaction mixture.[17,18] Tuning of the geometry, enforced by the ligand L, and variation of the anions added to the solution may lead to a range of polynuclear complexes with widely varied structural, electronic, and magnetic properties and the possibility of tuning the magnetic anisotropy.[18,19]

Another type of well characterized cyanometalate assembly is based on complexes with two free coordination sites $[M^b(L)_y(solvent)_2]^{k+}$. Examples have been published with $M^b = Ni^{2+}$ and hexacyanometalate(III) complexes with various anions A^- and cations C^+, which yield structures with interesting magnetic properties: $[\{Ni(L)_y\}_3\{M^a(CN)_6\}_2]\cdot x\,H_2O$,[20] $[\{Ni(L)_y\}_2\{M^a(CN)_6\}][A]\cdot x\,H_2O$,[21] and $[C][\{Ni(L)_y\}\{M^a(CN)_6\}]\cdot x\,H_2O$.[22] Depending on the ligand L, these assemblies have 2D "honeycomb" or "brick wall" or 1D "chain" structures. Aesthetically appealing 3D assemblies were built with ligands L blocking three out of the six sites in the coordination sphere of the metal ion M^b.[23–25] Magnetically interesting 3D clusters with bidentate ligands L have also been observed.[26]

The ligand L which blocks part of the coordination sites of the metal ion M^b, used to encapsulate the cyanometalates, may take part in intermolecular interactions, thus opening up further possibilities to influence the structure and properties of the polymetal assemblies. A promising approach is to use macrocyclic ligands with appended functional groups.[27] For example, complexes of Ni^{2+} with 3,10-dihydroxyethyl-1,3,6,8,10,12-hexaazacyclotetradecane have been used successfully for self-assembled structures which involve cyanometalates.[28–30] These structural motifs are basically identical to the corresponding nonfunctionalized assemblies,[31–33] but the magnetic behavior may be strongly influenced by secondary interactions. Modification of the macrocyclic ligands L also offers the possibility of producing structurally unusual assemblies.[34]

Reaction of the tris-macrocyclic ligand tricopper(II) complex $[Cu_3(L)]^{6+}$ (Figure 1) and $[Fe(CN)_6]^{4-}$ leads to the formation of the unusual octanuclear, water-soluble host–guest complex $[\{Cu_3(L)\}_2\{Fe_2(CN)_{11}\}]^{5+}$, which is formed by dimerization of the kinetically inert hexacyanoferrate(II) in the cavity of the tris-macrocyclic ligand tricopper(II) host complex.[35] Here, we report our investigation of the interaction of $[Cu_3(L)]^{6+}$ with $[M(CN)_6]^{3-}$ ($M = Cr^{3+}$, Mn^{3+}, Fe^{3+}, Co^{3+}) and $[M(CN)_8]^{4-/3-}$ ($M = Mo^{4+/5+}$, $W^{4+/5+}$) under similar reaction conditions. The structural properties of the resulting assemblies are reported in detail and an overview of the magnetic properties, based on temperature- and field-dependent data, as well as a first-order ligand field model, are also presented.

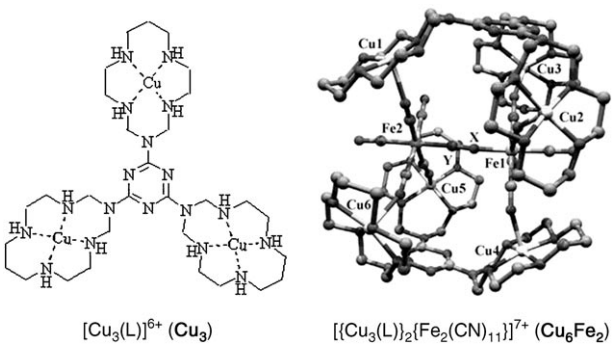

Figure 1. Structures of Cu_3 and Cu_6Fe_2.

Results and Discussion

Syntheses and spectroscopic properties: The mixed-anion salt $[Cu_3(L)](NO_3)_3(ClO_4)_3\cdot 2H_2O$ (Cu_3)[35] was found to be the most readily purified source for the tris-macrocyclic copper(II) host and was used in all experiments. The complexation of $[Cu_3(L)]^{6+}$ with $K_3[M(CN)_6]$ ($M = Cr^{3+}$, Fe^{3+}, Co^{3+}) was carried out in a hot aqueous solution of $NaNO_3$ ($1\,mol\,L^{-1}$), that is, under the conditions which lead to $[\{Cu_3(L)\}_2\{Fe_2(CN)_{11}\}]^{5+}$ (Cu_6Fe_2) in the reaction of $[Cu_3(L)]^{6+}$ with $K_4[Fe(CN)_6]$. After slow cooling of the reaction mixtures, crystalline precipitates of general composition $[\{Cu_3(L)\}\{M(CN)_6\}_2]\cdot 17H_2O$ were obtained. These products are insoluble in water, ethanol, acetone, acetonitrile, nitromethane, DMF, DMSO, and mixtures of these solvents; they are also insoluble in aqueous solutions of the corresponding hexacyanometalate anions (in up to tenfold excess). Crystals obtained in these experiments were generally of poor quality, but an X-ray structure determination was successful for the corresponding Cr^{3+} complex. According to the structural data, the Cr^{3+} host–guest assembly has the stoichiometry $[\{[Cu_3(L)(OH_2)_2][Cr(CN)_6]\}_2\{Cr(CN)_6\}]\cdot[Cr(CN)_6]\cdot 30H_2O$ (Cu_6Cr_4). Crystals of the corresponding Fe^{3+} (Cu_6Fe_4) and Co^{3+} (Cu_6Co_4) complexes were not of good enough quality for a full structural analysis, but they have the same stoichiometry and give X-ray powder diffraction patterns which are similar to that of the Cr^{3+} assembly (Figure 2a). Therefore, all three compounds (Cu_6Cr_4, Cu_6Fe_4, Cu_6Co_4) are considered to be isostructural. Isostructural complexes based on $[M(CN)_6]^{3-}$ ($M = Cr^{3+}$, Mn^{3+}, Fe^{3+}, Co^{3+}) have also been found with various other ligand systems.[20,22,36]

$[Mn(CN)_6]^{3-}$ is hydrolytically unstable in hot aqueous solution. Therefore, for a host–guest assembly with Mn^{3+} we were forced to use another synthetic procedure, namely vigorous stirring of the solid $K_3[Mn(CN)_6]$ in an ice-cold solution of $[Cu_3(L)]^{6+}$; the same procedure was subsequently used in experiments with $K_3[Cr(CN)_6]$ and $K_3[Fe(CN)_6]$. The resulting solid products consisted of very small crystals that could not be readily separated by filtration, so they were isolated by centrifugation. These samples, Cu_6Cr_4[a], Cu_6Fe_4[a], Cu_6Mn_4, and Cu_6Co_4[a] for Cr^{3+}, Fe^{3+}, Mn^{3+}, and Co^{3+}, respectively, have the same stoichiometry as the Cu_6Cr_4 and Cu_6Fe_4 samples obtained from hot aqueous solu-

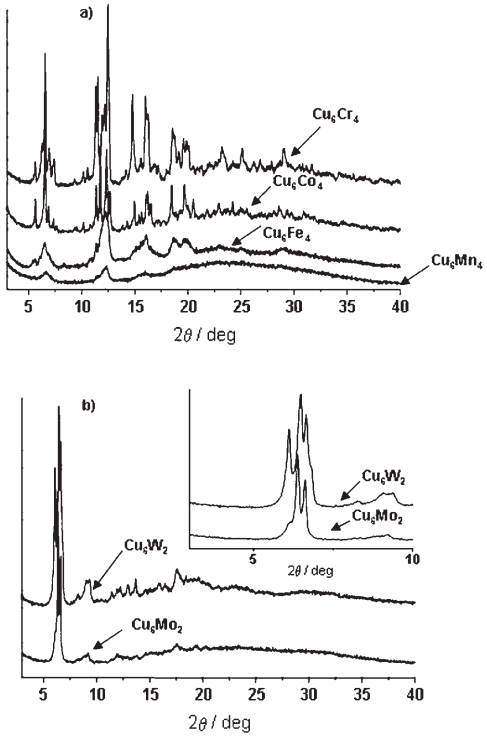

Figure 2. X-ray powder diffraction spectra: a) host–guest complexes of hexacyanometalate(III) guests; b) octacyanometalate(IV) host–guest complexes.

tion. Also, the magnetic behavior (see below) of related samples, **Cu_6Cr_4/Cu_6Cr_4**[a] and **Cu_6Fe_4/Cu_6Fe_4**[a], is identical; this result suggests that there is only one magnetic phase per metal ion. Evidence that the Mn^{3+} host–guest assembly **Cu_6Mn_4** is isostructural with the complexes with Cr^{3+}, Fe^{3+}, and Co^{3+} (**Cu_6Cr_4**, **Cu_6Fe_4**, **Cu_6Co_4**) emerges from the corresponding powder X-ray diffraction spectra (see Figure 2a). Although, due to the poor crystallinity of the samples, the intensity of the reflections is low in the spectra of the Fe^{3+} and Mn^{3+} assemblies, the reasonably well-resolved maxima are at the same angles as the peaks in the spectra of the corresponding Cr^{3+} and Co^{3+} samples. With Fe^{3+}, the samples of the host–guest assembly obtained from hot solution (**Cu_6Fe_4**) were contaminated with Fe^{2+}. This emerges from their IR spectra (ν_{CN}: **Cu_6Fe_4** 2109, 2114, 2040 cm^{-1}; $[Fe(CN)_6]^{4-}$ 2042 cm^{-1};[37] **Cu_3Fe_2** 2035 cm^{-1};[35] see Table 1). The samples obtained at low temperature (**Cu_6Fe_4**[a]) were free from traces of Fe^{2+}. The reduction of Fe^{3+} must be due to the interaction with the $[Cu_3(L)]^{6+}$ host and leads to a water-soluble complex, probably the known **Cu_3Fe_2**.[35]

The stoichiometry of the cyanometalate host–guest assemblies which result from the reaction of $[M(CN)_8]^{4-/3-}$ (M = $Mo^{4+/5+}$, $W^{4+/5+}$) with the $[Cu_3(L)]^{6+}$ host depends on the relative concentrations of the cyanometalate and of NO_3^- in the aqueous solution of the $[Cu_3(L)]^{6+}$ host. Without addition of $NaNO_3$, $[Cu_3(L)]^{6+}$ and $K_4[M(CN)_8]\cdot 2H_2O$ form stable solutions in water up to a ratio of 10:1 ($\{[Cu_3(L)]^{6+}\} = 4\times10^{-3}$ mol L^{-1}). In these solutions coordination of the cyanometalates to the tricopper(II) host was observed spectrophotometrically by the bathochromic shift of the Cu^{2+} d–d transition (19100 cm^{-1} versus ~18000 cm^{-1} for the free host and the host–guest complex, respectively; Table 1). With an increasing ratio of $[M(CN)_8]^{4-}$ (up to 10:3) considerable opalescence, attributable to the formation of insoluble products, was observed. Due to gel formation, however, it was not possible to collect this solid when no $NaNO_3$ was added. Well shaped, small, needle-like crystals of stoichiometry $[\{Cu_3(L)\}\{M(CN)_8\}](NO_3)_2\cdot 10H_2O$ were obtained when $[Cu_3(L)]^{6+}$ and $[M(CN)_8]^{4-}$ were allowed to react in hot aqueous $NaNO_3$ solution (1 mol L^{-1}). According to X-ray powder diffractograms, these assemblies with Mo^{4+} and W^{4+} are isostructural (Figure 2b). It was not possible to recrystallize them from water, water/DMF, or water/DMSO mixtures in order to get X-ray quality single crystals, because, upon stirring in these solvents, part of the $[Cu_3(L)]^{6+}$ host was dissolved (an electronic transition at 19100 cm^{-1} showed that the host–guest complexes were not stable) and a new, uncharacterized, insoluble phase (presumably with a host/guest ratio $[Cu_3(L)]^{6+}$:$[M(CN)_8]^{4-}$ of 2:3) was formed. This demonstrates the importance of NO_3^- for the stabilization of the crystal lattice and formation of specific assemblies.

For X-ray quality crystals of host–guest assemblies with $[M(CN)_8]^{3-/4-}$ (M = Mo, W), the starting materials were allowed to diffuse in a test tube (15 × 1.5 cm) that contained an aqueous solution with a gradient of $NaNO_3$. At the bottom of the test tube was a solution of the host complex $[Cu_3(L)]^{6+}$ in saturated aqueous $NaNO_3$; the second layer was an aqueous solution of $NaNO_3$ (1 mol L^{-1}), and the

Table 1. Spectroscopic and magnetic data of the cyanometalate complexes of $[Cu_3(L)]^{6+}$.

	IR $\tilde{\nu}$ [cm^{-1}]		UV/Vis $\tilde{\nu}$[a] [10^{-3} cm^{-1}]		$\chi_m T$[b] [emu K mol^{-1}]		M [$N_A\beta$]	
	$\nu_{(NCN)\,melamine}$	$\nu_{(CN)\,cyanometalate}$	d–d (Cu^{2+})	other bands	exptl	calcd (g_e = 2.00)	exptl	calcd (g_e = 2.00)
$(Cu_3)_2$	1566	–	19.1	33.3	2.40	2.25	5.81	6.00
Cu_6Cr_4	1567	2122, ~2128[c]	18.9	25.9; 33.3	10.15	9.75	16.69	18.00
Cu_6Fe_4	1569	2109, ~2114[c]	18.4	6.4; 23.1; 30.9	5.03	3.75	9.63	10.00
Cu_6Co_4	1570	2120, ~2128[c]	19.0	33.3	2.78	2.25	6.07	6.00
Cu_6Mn_4	1566	2106	19.0	12.4; 24.3; 30.1; 33.3	8.73	6.25	7.28	14.00
Cu_6Mo_2	1567	2104	17.9	26.6; 33.1	2.46	2.25	5.93	6.00
Cu_6W_2	1566	2098, 2156[d]	18.1	26.6; 32.6	2.39	2.25	5.72	6.00
Cu_6Fe_2	1564	2035	15.5	29.8	2.59	2.25	6.28	6.00

[a] T = 298 K. [b] T = 1.8 K. [c] Shoulder. [d] Low-intensity peak.

third was a solution of $[M(CN)_8]^{4-}$ in pure water. Two types of crystals were obtained after approximately 20 days. The first were needle-shaped crystals, with the same stoichiometry as observed without diffusion (see above), $[\{Cu_3(L)\}\{M(CN)_8\}](NO_3)_2\cdot 10H_2O$. These, according to the crystallographic data (see below), have two structurally independent octacyanometalate sites and may be described as $[\{[Cu_3(L)]_2[M(CN)_8]\}\{M(CN)_8\}](NO_3)_4\cdot 20H_2O$, that is, $\mathbf{Cu_6Mo_2}$ for Mo^{4+} and $\mathbf{Cu_6W_2}$ for W^{4+}. The second type of crystals are block-shaped with the stoichiometry $[\{Cu_3(L)(OH_2)\}_2\{Mo(CN)_8\}](NO_3)_8\cdot 15H_2O$, that is, $\mathbf{Cu_6Mo}$ for Mo^{4+} and $\mathbf{Cu_6W}$ for W^{4+}. Identical products were obtained, independently of the oxidation state of the starting material ($[M(CN)_8]^{3-/4-}$, M = Mo, W). Even in the dark, only complexes of Mo^{4+} and W^{4+} were obtained when $[M(CN)_8]^{3-}$ was treated with $[Cu_3(L)]^{6+}$ in aqueous $NaNO_3$ solution. Other examples of this type of redox behavior are known from the literature.[38]

The infrared spectra of the heteronuclear assemblies are dominated by a strong signal at 1567 cm^{-1}. This signal results from the triazine ring, is assigned to a ν(NCN) vibration, and is characteristic of the tricopper(II) host. Vibrations assigned to the CN groups in $\mathbf{Cu_6Cr_4}$, $\mathbf{Cu_6Fe_4}$, $\mathbf{Cu_6Co_4}$, $\mathbf{Cu_6Mn_4}$, and $\mathbf{Cu_6Fe_2}$[35] appear at lower frequencies than the corresponding potassium salts of the cyanometalates (2122, 2109, 2120, 2106, 2035 cm^{-1} for the host–guest complexes and 2128, 2118, 2129, 2120, 2040 cm^{-1} for the hexacyanometalates with Cr^{3+}, Fe^{3+}, Co^{3+}, Mn^{3+}, and Fe^{2+}, respectively[37]). The host–guest complexes of the octacyanometalates, in contrast to the corresponding starting materials, $K_4[M(CN)_8]\cdot 2H_2O$ (M = Mo, W), also have an infrared transition due to the CN vibrations. These appear at 2104 and 2098 cm^{1-}, respectively, and are probably superimpositions of several transitions due to bridging CN groups in the octacyanometalate anions[38] in different sites of the crystal lattice.

The d–d transitions of the copper(II) centers of the "free" tris-macrocyclic host ($\mathbf{Cu_3}$) appear at 19100 cm^{-1} (see Table 1 and Figure 3).[39,40] This transition is shifted to lower energy in the heteronuclear complexes (strong axial donors reduce the transition energy). The largest shift is found for $\mathbf{Cu_6Fe_2}$ ($\tilde{\nu}_{max} = 15500\ cm^{-1}$), in which all the Cu^{2+} ions have relatively short axial bonds to nitrogen atoms of the $[Fe_2(CN)_{11}]^{7-}$ host; also, considerable distortion of the CuN_4 plane in this example further reduces the ligand field. Much smaller shifts are observed for the host–guest assemblies with Mo^{4+} and W^{4+} ($\mathbf{Cu_6Mo_2}$ and $\mathbf{Cu_6W_2}$), for which the observed transition energies are at 17900 and 18100 cm^{-1}, respectively. This is expected from the crystal structure of the W^{4+} complex ($\mathbf{Cu_6W_2}$) (vide infra), which shows that distortions of the Cu^{2+} chromophores are relatively small, in spite of rather short bonds to the axial donors. Even smaller shifts of the Cu^{2+} d–d transitions are observed for the hexacyanometalate(III) assemblies, which have transitions at 18900, 18450, and 19000 cm^{-1} for the Cr^{3+}, Fe^{3+}, and Co^{3+} assemblies, respectively. The Cu^{2+} d–d transitions of the Mn^{3+}complex $\mathbf{Cu_6Mn_4}$ overlap with charge transfer transitions and bands originating from the hexacyanomanganate core.

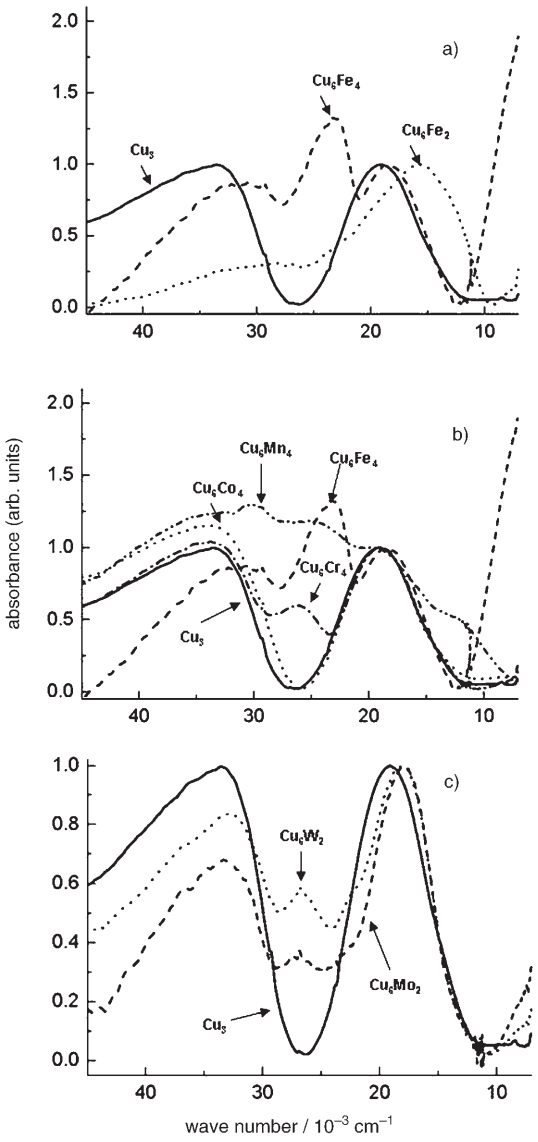

Figure 3. UV-visible diffused reflectance spectra.

The EPR spectra of solid samples of the host–guest complexes show a broad unresolved signal with $g \approx 2.09$, assigned to the Cu^{2+} ions (see Supporting Information). This signal is very weak and difficult to detect in paramagnetic cyanometalate host–guest complexes (M = Cr^{3+}, Fe^{3+}), but it supports the oxidation state assigned to the metal ions involved.

Molecular and crystal structures of the bimetallic assemblies: The Cu^{2+} ions in all the structures are coordinated to the four nitrogen donors of the cyclam-derived macrocycles, resulting in nearly planar CuN_4 chromophores (rms = 0.01–0.04 Å; Table 2), with the Cu^{2+} centers only slightly displaced from from these planes (by 0.01–0.07 Å). The coordinated pentaazamacrocycles have the expected *trans*-III

Table 2. Selected bond lengths [Å] and angles [deg] for the cyanometalate complexes of $[Cu_3(L)]^{6+}$.

	Cu_6Cr_4	Cu_6Mo	Cu_6W_2	Cu_6Fe_2[a]
Cu···Cu	7.61 (Cu1−Cu2][b]	8.15 (Cu2−Cu3)[b]	7.59 (Cu1−Cu2)[b]	7.51 (Cu4−Cu6)[b]
	8.15 (Cu2−Cu3)[b]	8.48 (Cu1−Cu2)[b]	8.25 (Cu6−Cu4)[b]	8.22 (Cu1−Cu3)[b]
		7.67 (Cu1−Cu2a)[c]	7.49 (Cu6−Cu2)[c]	8.04 (Cu1−Cu6)[c]
		10.02 (Cu3−Cu3a)[c]	8.26 (Cu3−Cu4)[c]	10.13 (Cu1−Cu5)[c]
		7.19 (Cu1−Cu3a*)[d]	7.45 (Cu1−Cu2a)[d]	
Cu ··· M	5.30 (Cu2−Cr1)	5.26 (Cu2−Mo1)	5.42 (Cu6−W2)	5.13 (Cu4−Fe1)
	5.35 (Cu3−Cr2)	5.29 (Cu1−Mo1)	5.84 (Cu4−W2)	5.20 (Cu2−Fe1)
	5.41 (Cu2−Cr2)	7.28 (Cu3−Mo1)	5.37 (Cu5−W1)	5.13 (Cu4−Fe2)
				5.28 (Cu6−Fe2)
M ··· M′	8.86 (Cr1−Cr3)	13.17	10.79–11.14	4.96
	10.50 (Cr1−Cr2)			
Cu−NH	1.974–2.030	2.016–2.047	1.970–2.053	1.968–2.033
Cu−NC	2.247	2.296; 2.309	2.171–2.568	2.201–2.263
$Cu-OH_2$	2.346, 2.349	2.404–2.637	≥2.99	–
N≡C	1.114–1.173	1.148–1.165	1.140–1.209	–
NC−M	2.024–2.092	2.154–2.174	2.068–2.195	1.893–1.927
Cu−N≡C	153.4	141.3; 141.9	141.6–165.6	149.2–163.5
$N-Cu-OH_2$	91.6–94.4	82.1–95.7	–	–
N−Cu−NC	93.5–95.4	91.7–95.2	87.4–99.0	86.4–106.2
N−Cu−N[e]	84.7–86.8	85.0–85.9	84.0–86.8	84.2–86.4
	93.5–94.7	92.5–94.8	90.8–98.3	90.1–96.2
N≡C−M	173.2–179.0	175.5–177.0	174.3–178.7	173.3–179.7
C−M−C	86.7–96.2	71.1–78.0	69.9–87.3	85.9–93.4
Cu−N≡C-M	15.0	−26.1; 44.5	9.2–162.0	1.8–117.5

[a] Reference [35]. [b] Shortest and longest distance within an individual $[Cu_3(L)]^{6+}$ structure. [c] Shortest and longest distance within the $[Cu_3(L)]_2^{6+}$ cage. [d] Shortest distance in the crystal lattice between atoms from different molecular units. [e] For five- and six-membered rings.

(*RRSS*) configuration[41] the tricopper(II) complexes adopt a *syn*,*syn* conformation, and the structural parameters of the CuN_4 chromophores are as expected.[42]

*[{[Cu_3(L)$(OH_2)_2$][$Cr(CN)_6$]}$_2${$Cr(CN)_6$}][$Cr(CN)_6$]·30 H_2O (**Cu_6Cr_4**)*: One $[Cr(CN)_6]^{3-}$ ion is located inside the cavity of the tricopper(II) host (Figure 4). The distances between the copper(II) center and the nitrogen donors of CN^- are long (3.45–3.86 Å), and the corresponding angles (N_{amine}-Cu-N_{CN}, 50.8–60.7°) deviate from those expected for axial coordination. The closest contacts are between the nitrogen atoms of the CN^- groups and the secondary amines of the neighboring macrocycles (2.98–3.03 Å), and this is probably due to hydrogen bonds and electrostatic interactions, which may be the main driving force for the formation of these assemblies.

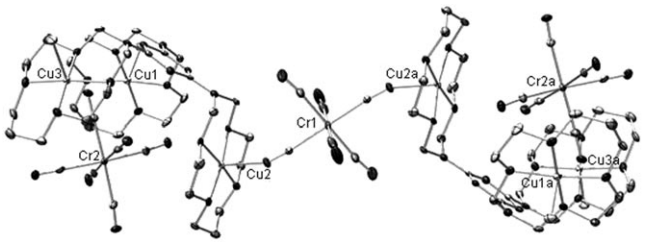

Figure 4. ORTEP plot (20% probability ellipsoids) of the **Cu_6Cr_4** molecular subunit; hydrogen atoms, noncoordinating hexacyanochromate(III) anion, and lattice solvent molecules are omitted for clarity.

The axial sites of the copper(II) ions on the outside of the cavity of the tris-macrocyclic tricopper(II) unit remain accessible for coordination. For two of the Cu^{2+} centers these are occupied by water molecules at approximately 2.35 Å (typical for five-coordinate, square-pyramidal axial OH_2 sites), and the third copper(II) ion coordinates to $[Cr(CN)_6]^{3-}$ (r(Cu−NC) = 2.248 Å), which leads to a bridge between two structurally identical host cavities (Figure 4). The third, structurally independent, hexacyanochromate(III) anion is not coordinated to any Cu^{2+} center, but takes part in the formation of an extended hydrogen-bond network, which includes secondary amines of the macrocycles and clathrated molecules of water (see Supporting Information). All three cyanochromate anions are octahedral, with distances and angles as expected for $[Cr(CN)_6]^{3-}$ (see Table 2).[43]

*[{Cu_3(L)(OH_2)}$_2${$Mo(CN)_8$}]$(NO_3)_8$·15 H_2O (**Cu_6Mo**)*: This compound crystallizes in the *C*2/*c* space group, and contains an Mo center in a special position (twofold axis). This leads to a structure of the assembly with isolated spheres (Figure 5). The $[Mo(CN)_8]^{4-}$ ion, with typical distances and angles (Table 2),[43] is coordinated to four of the six available Cu^{2+} ions (r(Cu−NC) = 2.296 Å and 2.309 Å). The CN^- groups not coordinated to Cu^{2+} centers are connected by hydrogen bonds to the N−H donors of the macrocyclic ligands or to water molecules (O2), which are axially coordinated to the other Cu^{2+} centers (Cu3 and Cu3a). This coordination mode is probably due to the relatively small size of the octacyanomolybdate(IV) anion. The arrangement of nitrate anions and water molecules outside the spherical host–guest structure is severely disordered. The *exo*-axial positions of the Cu^{2+} centers are occupied by water molecules (Cu2−O4) or by a nitrate donor (N23−O), which connects the adjacent spheres; these contacts are weak (r(Cu−O) = 2.570 and 2.605 Å). The structure of the analogous tungsten complex (**Cu_6W**) is qualitatively similar but, because of low crystal quality, the data are scarce and the structural parameters cannot be published.

*[{[Cu_3(L)]$_2$[$W(CN)_8$]}{$W(CN)_8$}]$(NO_3)_4$·20 H_2O (**Cu_6W_2**)*: A similar structural motif to that of **Cu_6Mo** described above is present in the host–guest complex **Cu_6W_2**. It consists of two structurally independent $[W(CN)_8]^{4-}$ units. One is coordinat-

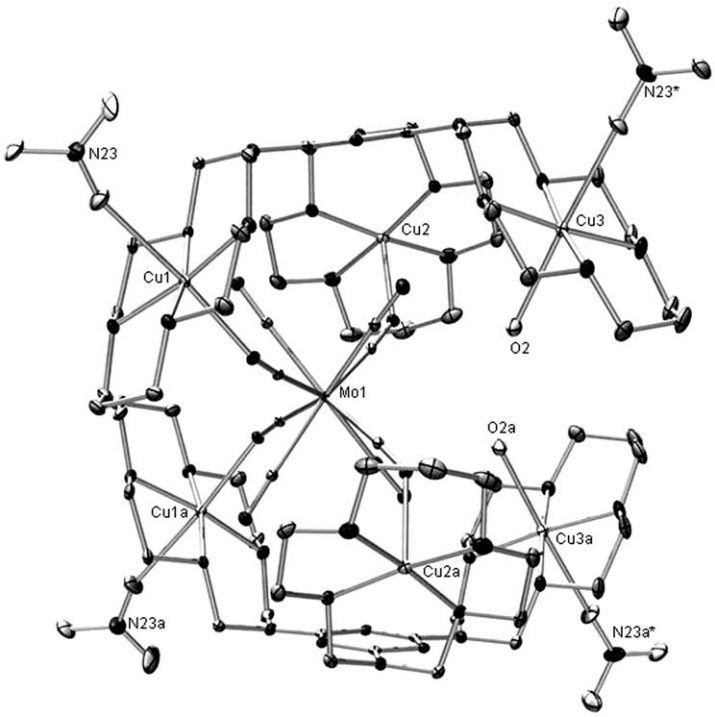

Figure 5. ORTEP plot (20% probability ellipsoids) of the **Cu_6Mo** molecular subunit; hydrogen atoms, noncoordinating nitrate anions, and lattice solvent molecules are omitted for clarity.

ed inside a $\{[Cu_3(L)]_2\}^{12+}$ cage, the other has a special position on the outside of the $[\{Cu_3(L)\}_2\{W(CN)_8\}]^{8+}$ complex (Figure 6). The encapsulated W^{4+} center is connected by CN^- bridges to four Cu^{2+} ions (r(Cu–NC) = 2.175, 2.212, 2.306, and 2.568 Å). In contrast to **Cu_6Mo**, there are no water molecules coordinated to the Cu^{2+} centers inside the cage. Also, the distances to the axial donors outside the cage (water molecules and nitrate anions) are long ($\geq$2.99 Å). The encapsulated $[W(CN)_8]^{4-}$ units are closer to the center of the spherical host–guest structure than in the structure of **Cu_6Mo** above. The outside environment of **Cu_6W_2** consists of three structurally equivalent $[W(CN)_8]^{4-}$ units (Figure 6), coordinated in different structural modes to the copper(II) centers (r(Cu–NC) = 2.171, 2.271, and 2.441 Å). This results in a cyano-bridged system which consists of eight metal ions: (**Cu-**NC)$_3$-**W**-CN-**Cu**-NC-**W**-(CN-**Cu**)$_2$ (Figure 7a). Six copper(II) ions of the unit belong to three different molecules of the tris-macrocyclic host; this results in a 2D structure, which may be described as an "accordion"-like layer (Figure 7b).

A comparison of the structures of **Cu_6Cr_4**, **Cu_6W_2**, **Cu_6Mo**, and **Cu_6Fe_2**[35] may help to design new architectures of similar assemblies. Due to the triazine spacer, the tris-macrocyclic ligand copper(II) host $[Cu_3(L)]^{6+}$ may adopt one of two

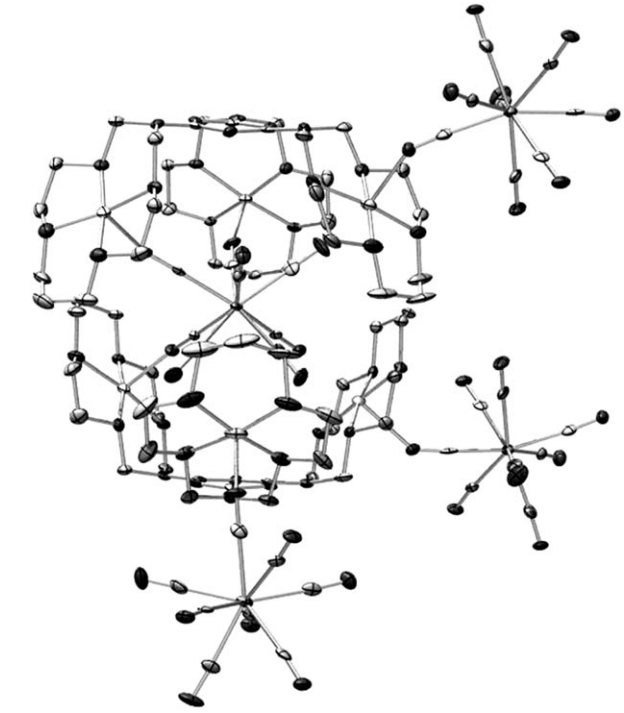

Figure 6. ORTEP plot (20% probability ellipsoids) of the **Cu_6W_2** molecular subunit; hydrogen atoms, nitrate anions, and lattice solvent molecules are omitted for clarity.

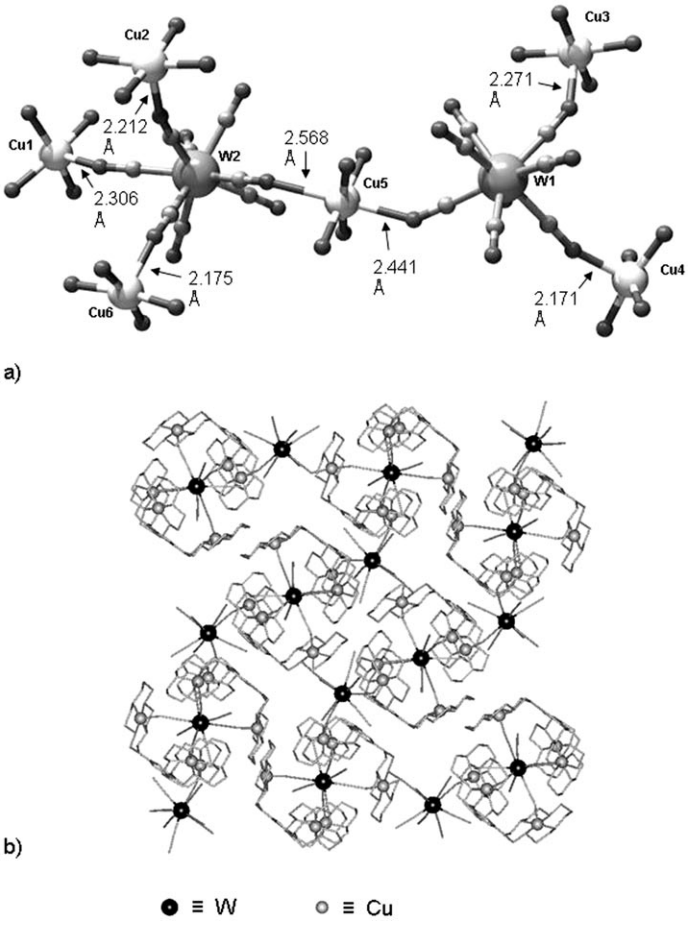

Figure 7. Structural plots of the part of the crystal lattice of **Cu_6W_2** demonstrating: a) cyano-bridged octanuclear unit; b) connectivity of the octacyanometalate and copper(II) complex in the layer (viewed from the top); hydrogen atoms, nitrate anions, and lattice solvent molecules are omitted for clarity.

energetically stable conformations: either *syn*,*anti*, in which the macrocyclic ligand copper(II) subunits are oriented on different sides of the plane of the aromatic spacer groups,[35,44,45] or *syn*,*syn*, in which all three macrocyclic ligand tricopper(II) subunits are on the same side.[35] The energy barrier between these two conformers seems to be small enough to be overcome in the free $[Cu_3(L)]^{6+}$ host in solution at ambient temperature.[35,44,45] Therefore, the structure of the host in the solid depends on the balance of various forces due to the crystal lattice. Our observations so far indicate that, upon interaction of the tricopper(II) host complex with cyanometalates, $[Cu_3(L)]^{6+}$ generally adopts the *syn*,*syn* conformation. The main factors responsible for this preference are probably the large negative charge and the relatively small size of the cyanometalates, which fit reasonably well into the spherical cavity of the host complex, and efficient charge neutralization is probably an important factor also. From the fact that the $\{[Cu_3(L)]^{6+}\}_2$ (**Cu_6**) host is able to induce the formation of $[Fe_2(CN)_{11}]^{7-}$ and to accommodate the dinuclear product, it follows that the size and shape of $[Fe_2(CN)_{11}]^{7-}$ complements those of the host cavity. This indicates that the host structure is quite flexible and that selectivity of size and shape is not the only factor and probably not the major one. The fact that the formation of the neutral assemblies $[\{Cu_3(L)\}\{M(CN)_6\}_2]$ ($M=Cr^{3+}$, Mn^{3+}, Fe^{3+}, Co^{3+}) is more favorable than the formation of $[\{Cu_3(L)\}_2\{M_2(CN)_{11}\}]^{7+}$ indicates how important electrostatic interactions are in these host–guest assemblies. The observation that two structural types are obtained with the octacyanometalates of Mo and W indicates that there is a subtle balance between a number of factors, including shape, size, electrostatic interactions, hydrogen bonding, and electronic effects, which as yet do not generally allow prediction of the relative stabilities of various minima with similar energy.

Magnetic properties: Temperature-dependent magnetic susceptibilities (χ) and field dependencies of the magnetizations (M, at 1.8 K) of the free host **Cu_3** and the host–guest complexes **Cu_6Cr_4**, **Cu_6Fe_4**, **Cu_6Co_4**, **Cu_6Mn_4**, **Cu_6Mo_2**, **Cu_6W_2**, and **Cu_6Fe_2** were measured in the temperature range 2–300 K. Figures 8 and 9 show the corresponding $\chi_m T$ versus T and M versus $\beta H/kT$ plots. Note that the magnetic behavior of **Cu_6Cr_4**[a] and **Cu_6Fe_4**[a] is identical to that of **Cu_6Cr_4** and **Cu_6Fe_4**, respectively. This indicates that, the two compounds are very probably isostructural, independent of their synthetic routes, and it suggests that the corresponding Mn^{3+} complex **Cu_6Mn_4** is also isostructural with the Cr^{3+} complex (**Cu_6Cr_4**), the structure of which has been determined experimentally. This also emerges from the X-ray powder patterns (see above).

Room-temperature values for $\chi_m T$, and for the magnetization M at $H=5$ T, together with the calculated values, based on spin-only formulas for noninteracting spins (room-temperature data), are listed in Table 1. There is good agreement between the total number of spins and the experiment, both for the free host complex **Cu_3** and the host–guest assemblies **Cu_6Co_4**, **Cu_6Mo_2**, **Cu_6W_2**, and **Cu_6Fe_2** with the non-

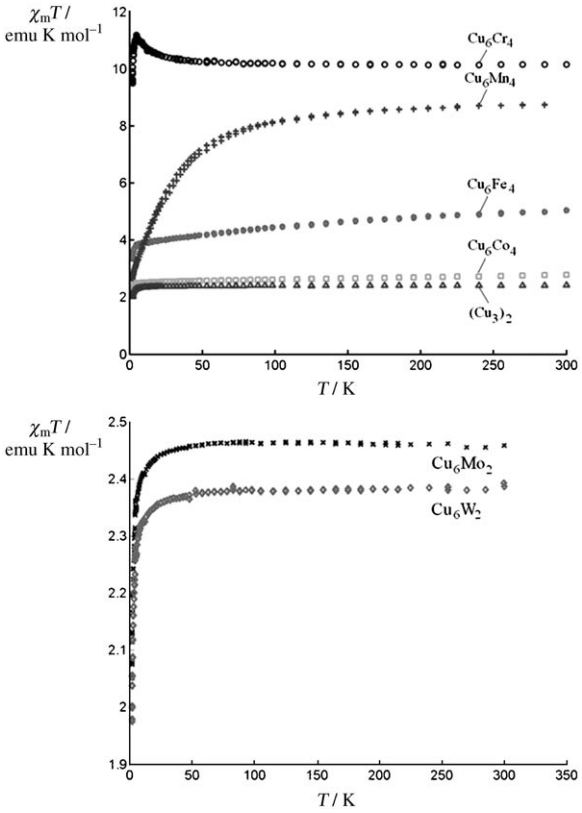

Figure 8. Plots of $\chi_m T$ versus T for the complexes **Cu_6Cr_4**, **Cu_6Fe_4**, **Cu_6Co_4**, **Cu_6Mn_4** and **Cu_3** (top); **Cu_6Mo_2** and **Cu_6W_2** (bottom). Values are calculated considering 2 mol of $[Cu_3(L)]^{6+}$ per assembly.

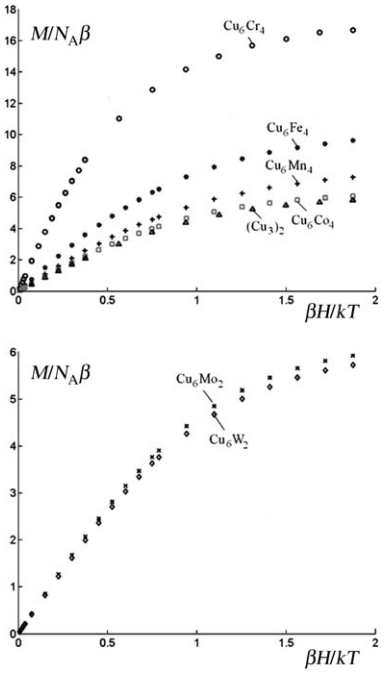

Figure 9. Dependence on the field [$\beta H/kT$ units], $T=1.8$ K, of the magnetization M ($N_A\beta$): top: **Cu_3**, **Cu_6Cr_4**, **Cu_6Fe_4**, **Cu_6Co_4**, and **Cu_6Mn_4**; bottom: **Cu_6Mo_2** and **Cu_6W_2**. Values are calculated considering 2 mol of $[Cu_3(L)]^{6+}$ per assembly.

magnetic (closed-shell) ions Co^{3+}, Mo^{4+}, W^{4+}, and low-spin Fe^{2+}. Good agreement with the spin count, corresponding to Cu^{2+} and Cr^{3+}, is also achieved for the complex **Cu_6Cr_4**, where the Cr^{3+} guest ion is in an orbitally nondegenerate $^4A_2$ ground state. However, for the assemblies with the low-spin $Fe^{3+}(d^5)$ **Cu_6Fe_4** and $Mn^{3+}(d^4)$ **Cu_6Mn_4** complexes the experimental $\chi_m T$ and M data are higher and lower, respectively, than their spin-only values. Orbital contributions to the magnetic properties, due to the orbitally degenerate octahedral $^2T_2(d^5)$ and $^3T_1(d^4)$ ground states, are essential here and need a more detailed analysis.

We first focus on the Cu^{2+}-only magnetic centers in **Cu_3**, **Cu_6Co_4**, **Cu_6Mo_2**, **Cu_6W_2**, and **Cu_6Fe_2**. There is a drop in the $\chi_m T$ versus T curves when temperatures close to 1 K are approached. This may be interpreted in terms of weak Cu···Cu antiferromagnetic coupling. Alternatively, it can be due to intermolecular interactions, which are neglected in our model calculations. Based on antiferromagnetic coupling with an equilateral triangular Cu_3 exchange cluster, a reasonable fit of the field-dependent magnetization curves is possible and yields Cu···Cu magnetic coupling constants J' of -0.45, -0.10, and $-0.40\ cm^{-1}$ (exchange Hamiltonian $H_{exc} = -J_{12}\cdot S_1\cdot S_2$) for **$Cu_3$**, **$Cu_6Co_4$**, and **$Cu_6Mo_2$**, respectively. An alternative interpretation, assuming a ferromagnetic Cu···Cu coupling and exchange anisotropy terms, is less plausible because of the weakness of the Cu···Cu interactions.

Antiferromagnetic Cu···Cu interactions are superimposed by the much stronger Cu···Cr coupling in **Cu_6Cr_4**. The rise in the $\chi_m T$ versus T plot (Figure 8 top) at T below 50 K indicates a significant ferromagnetic Cu ($s = 1/2$)···Cr ($s = 3/2$) spin–spin interaction. With a two-parameter model and the exchange topology shown in Figure 10 (top), a good fit to both the susceptibility (Figure 10, middle) and magnetization curve (Figure 10, bottom) was possible. This allows values of the Cu···Cr ($6.8\ cm^{-1}$) and Cu···Cu ($-1.9\ cm^{-1}$) exchange integrals to be deduced. The latter is significantly stronger than the coupling which emerges from **Cu_3**, **Cu_6Co_4**, **Cu_6Mo_2** and **Cu_6W_2** (see above).

The ferromagnetic interaction between Cu^{2+} and Cr^{3+} can be rationalized by a charge transfer mechanism as shown in Figure 11. The transfer of a beta spin from fully occupied orbitals of π symmetry at Cu to the singly occupied t_{2g} π orbitals of Cr^{3+} leads to a triplet excited state configuration on Cu^{2+}. This becomes stabilized against a local singlet charge-transfer state due to intraatomic exchange (Hund) at $Cu^{3+}(d^8)$. In the complex considered here, the Cu-NC-Cr bridging geometry is not linear. Antiferromagnetic exchange pathways due to this nonlinearity possibly contribute as well. However, they cannot outweigh the dominant ferromagnetic Cu^{2+}···Cr^{3+} coupling.

To interpret the magnetic data of complexes **Cu_6Fe_4** and **Cu_6Mn_4**, additional experiments and proper analyses of the magnetic behavior of the $[Fe(CN)_6]^{3-}$ and $[Mn(CN)_6]^{3-}$ building blocks in their $^2T_2$ and $^3T_1$ states were needed. Therefore, we recorded magnetic susceptibility and magnetization data of the $[M(CN)_6]^{3-}$ species in $[(Ph_3P)_2N]_3[M(CN)_6]\cdot x\,H_2O$ ($M = Fe^{3+}$, Mn^{3+}).[46] Due to the large cations and the emerging separation of the hexacyanometalates in the lattice, there is only weak coupling between the paramagnetic $[M(CN)_6]^{3-}$ units. The $\chi_m T$ versus T and magnetization M versus $\beta H/kT$ data (Figures 12 top and bottom, respectively) could be fitted nicely in terms of a two-parameter model, which involves the spin–orbit coupling constant and the orbital reduction factor, and assumes cubic geometries for $[Mn(CN)_6]^{3-}$ and $[Fe(CN)_6]^{3-}$. There is no indication of any pronounced Jahn–Teller activity on the basis of our powder data. However, small ground-state splitting due to Jahn–Teller and/or lattice strain distortions may show up in anisotropic magnetic behavior, and may be amenable to

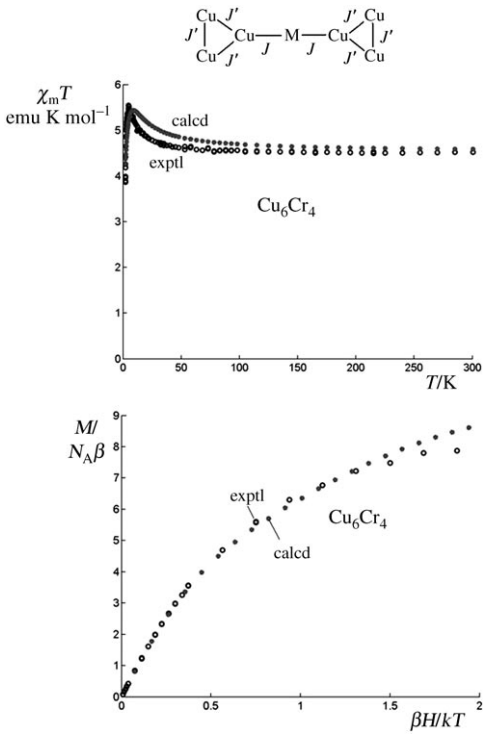

Figure 10. Top: Topology of the exchange interaction adopted to fit the magnetic data for **Cu_6Cr_4**. Middle: Experimental and simulated $\chi_m T$ versus T for the **Cu_6Cr** fragment in **Cu_6Cr_4**. Experimental points refer to χ_m. T values were obtained from the magnetic susceptibility of **Cu_6Cr_4** after subtracting contributions due to three weakly coupled $[Cr(CN)_6]^{3-}$ centers [$3\times 0.125\,05 g_e^2 S(S+1)$, $S = 3/2$]. Bottom: Experimental and simulated field dependence of the magnetization for **Cu_6Cr_4**. Best-fit values of the Cu–Cu and Cu–Cr exchange integrals adopted for the simulated curves are 6.8 and $-1.9\ cm^{-1}$, respectively.

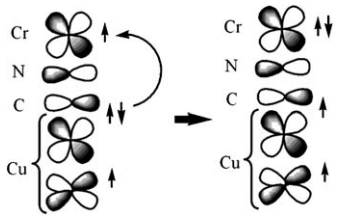

Figure 11. Exchange mechanism rationalizing the ferromagnetic Cu–Cr coupling for **Cu_6Cr_4**.

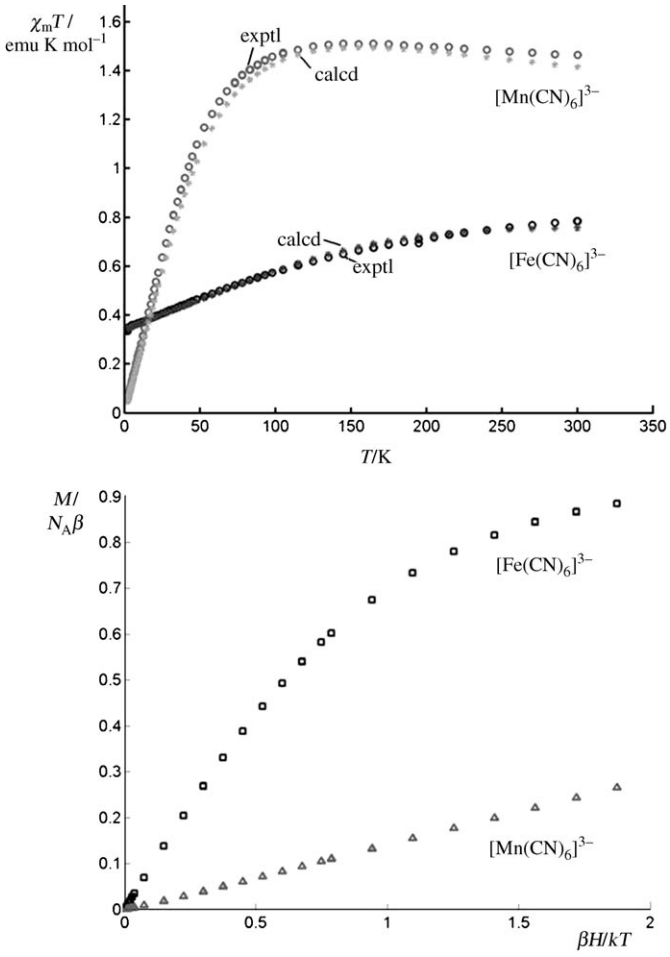

Figure 12. Top: Plots of $\chi_m T$ versus T ($H=0.1$ T) for the complexes $[Fe(CN)_6]^{3-}$ and $[Mn(CN)_6]^{3-}$ in $[(Ph_3P)_2N]_3[M(CN)_6]\cdot x H_2O$ ($M=Fe^{3+}$, Mn^{3+}). Calculated data, using best-fit values of the spin–orbit coupling constant ζ and the orbital reduction factor k are included; $\zeta(k)=-123\ cm^{-1}$ (0.913) and $-274\ cm^{-1}$(0.93) for $M=Mn^{3+}$(g=1.95) and Fe^{3+} (g=2.00). respectively; Bottom: dependence of the field [$\beta H/kT$ units], $T=1.8$ K), of the magnetization M [$N_A\beta$] for $[Fe(CN)_6]^{3-}$ and $[Mn(CN)_6]^{3-}$ in $[(Ph_3P)_2N]_3[M(CN)_6]\cdot x H_2O$ ($M=Fe^{3+}$, Mn^{3+}).

measurements on single crystals. These will be discussed elsewhere. In octahedral coordination the $^2T_2$ and $^3T_1$ ground states of octahedral Fe^{3+} and Mn^{3+} are split by spin–orbit coupling. The resulting mutiplet components and their effective g values (g_{eff}) are represented schematically in Figure 13. At very low temperatures only Γ_8 and A_1 are occupied. The latter state is diamagnetic, while at higher temperatures a Kramers doublet is thermally populated. However, some reduction of the effective g-tensor value ($g_{eff}=2.0023$), due to covalency ($k<1$) takes place. The g tensors in Figure 13 quantify the expected changes in the magnetic moments when higher multiplet states become thermally occupied. These moments increase for Mn^{3+} with increasing temperature, starting from zero for $T=0$ K, and are modified, but to a lesser extent, by temperature in the case of the Fe complex **Cu_6Fe_4** also.

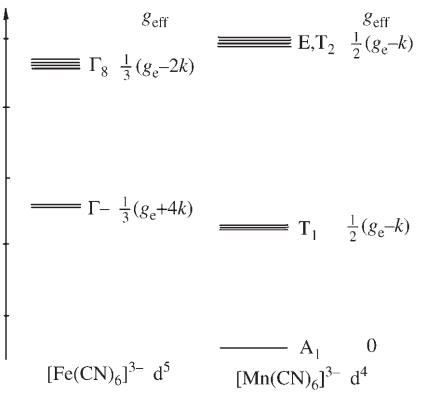

Figure 13. Multiplet fine structure due to the spin–orbit splitting of the $^2T_2(d^5)$ and $^3T_1(d^4)$ ground states of octahedral $[Fe(CN)_6]^{3-}$ and $[Mn(CN)_6]^{3-}$, respectively.

Table 3. Room-temperature ($T=300$ K) magnetic susceptibilities ($\chi_m T$ [emu K mol^{-1}], $H=0.1$ T) and high-field ($H=5$ T) magnetization M [$N_A\beta$], $T=1.8$ K), of low-spin $[(Ph_3P)_2N]_3[M(CN)_6]\cdot x H_2O$ ($M=Fe^{3+}$, Mn^{3+}) including spin-only values of χT and M for $s=1/2$ ($s=1$) for low-spin octahedral Fe^{3+} (Mn^{3+}).

Complex	$\chi_m T$[a]		M[b]	
	exptl	calcd	exptl	calcd
$[Fe(CN)_6]^{3-}$	0.79	0.375	0.88	1
$[Mn(CN)_6]^{3-}$	1.46	1.00	0.26	2

[a] $H=0.1$ T, $T=300$ K. [b] $H=5$ T, $T=1.8$ K.

In Table 3 we summarize room-temperature values ($H=0.1$ T) of $\chi_m T$ and low-temperature ($T=1.8$ K) high-field values ($H=5$ T) of M for these two complexes. Spin-only values are also included for comparison. It is remarkable that the experimental data for $\chi_m T$ are lower, while the magnetization data M are higher, than the corresponding spin-only values ($S=1/2$ for Fe^{3+}, $S=1$ for Mn^{3+}). Thus, the trends in the $\chi_m T$ and M curves for the $Cu_3(L)\cdots Mn(CN)_6$ and $Cu_3(L)\cdots Fe(CN)_6$ complexes closely resemble those of the constituent $[Mn(CN)_6]^{3-}$ and $[Fe(CN)_6]^{3-}$ fragments. Indeed, comparison shows (see Supporting Information) that magnetization plots of $Cu_3(L)\cdots M(CN)_6$ almost coincide with the sum of the contributions due to $Cu_3(L)$ (using the compound Cu_6Co_4 as a reference) and $[M(CN)_6]^{3-}$ (taking experimental data for the $[(Ph_3P)_2N]_3[M(CN)_6]\cdot x H_2O$ ($M=Fe^{3+}$, Mn^{3+}) salts as references). This clearly shows that M···Cu exchange coupling in the complexes **Cu_6Fe_4** and **Cu_6Mn_4** (structures not determined by single-crystal diffraction studies) is very small and presumably weakly ferromagnetic in the case of M = Mn, and vanishingly small for M = Fe.

More detailed theoretical analyses of the magnetic exchange across the cyanide bridge, covering the systems considered here and including other interesting examples from the literature, will be reported separately.

Conclusions and Outlook

The tris-macrocyclic ligand tricopper(II) complex $[Cu_3(L)]^{6+}$ is an efficient host for a variety of cyanometalate assemblies. Due to the conformational flexibility the tris-macrocyclic host may adopt the *syn*,*anti* conformation, which may lead to a linear-chain type of structure or a bowl-shaped *syn*,*syn* conformation, suitable for the encapsulation of relatively small cyanometalate anions. The latter conformation leads to the stabilization of magnetically coupled octametal units in the case of hexacyanometalates bearing a charge of 3−, and to spherical assemblies with the octacyanometalates of Mo^{4+} and W^{4+}.

Magnetic susceptibility and magnetization data indicate that the magnetic exchange coupling between the paramagnetic centers is generally weak. It is weakly antiferromagnetic for the Cu···Cu pairs in the free host $[Cu_3(L)]^{6+}$ (**Cu_3**) and shows some dependence on the intervening transition–metal ion in the host–guest assemblies **Cu_6Co_4**, **Cu_6Mo_2**, and **Cu_6W_2** with closed-shell host complex centers. For the Cu···Cr pair (**Cu_6Cr_4**) a ferromagnetic Cu···Cr coupling takes place. The exchange is found to be small and nearly negligible for the Cu···Mn and Cu···Fe pairs in **Cu_6Mn_4** and **Cu_6Fe_4**, respectively. The Cu···Mo and Cu···W systems behave magnetically similarly to the free host complex $[Cu_3(L)]^{6+}$, since the eight-coordinate Mo^{4+} and W^{4+} are in a closed-shell ground state electronic configuration. Partial oxidation to Mo^{5+} and W^{5+} has been observed and is expected to proceed photochemically also, possibly to lead to photomagnetism, as has been demonstrated in other systems recently.[47,48]

Experimental Section

Measurements: Infrared spectra (KBr pellets) were recorded with a Perkin–Elmer 16 PC FT-IR spectrometer. UV-visible spectra were measured on a Jasco V-570 UV/VIS/NIR instrument (diffuse reflectance, PTFE pellets). EPR spectra were obtained with a Bruker ELEXSYS E500 spectrometer (X-band). X-ray powder diffraction experiments were performed using a Philips XPert diffractometer with $Cu_{K\alpha}$ radiation and a secondary beam monochromator. The scan rate was 0.008 deg s^{-1}. Samples were crushed in a mortar under ethanol and spread on glass slides. Magnetic measurements were performed in "zero-field-cold" mode (DC) using a Quantum Design MPMS XL magnetometer equipped with a 50 kG magnet and operating in the 300–1.8 K range. Powdered samples were kept in gelatin containers, and the data were corrected for diamagnetism of the container; Pascal's constants were used for diamagnetic correction of the samples.

Crystallography: Reflections of representative crystals were measured with Bruker AXS SMART 1000 (for **Cu_6Mo**) and STOE IPDS (for **Cu_6Cr_4** and **Cu_6W_2**) diffractometers with $Mo_{K\alpha}$ radiation ($\lambda = 0.71073$ Å), and operating in the ω-scan mode. The absorption correction was applied in all cases. The structures were solved by direct methods (SHELXS86) and refined by full-matrix, least-squares methods based on F^2 (SHELXL97), with use of anisotropic thermal parameters for all non-hydrogen atoms (see Table 4). CCDC 267422–267424 contain the supplementary crystallographic data for this paper. These data can be obtained free of charge from the CambridgeCrystallographic Data Centre via www.ccdc.cam.ac.uk/data_request/cif.

Table 4. Experimental results of the X-ray diffraction studies.

	Cu_6Cr_4	**Cu_6W_2**	**Cu_6Mo**
formula	$C_{42}H_{100}Cr_2Cu_3N_{30}O_{17}$	$C_{76}H_{172}Cu_6N_{56}O_{32}W_2$	$C_{68}H_{166}Cu_6N_{52}O_{41}Mo$
M_r	1592.14	3131.49	2845.71
T [K]	210(2)	210(2)	103(2)
crystal system	triclinic	monoclinic	monoclinic
space group	$P\bar{1}$	$P2_1/n$	$C2/c$
a [Å]	16.129(3)	19.127(4)	29.0042(19)
b [Å]	16.346(3)	26.519(5)	26.0604(17)
c [Å]	17.725(4)	27.398(6)	16.5273(11)
α [°]	88.38(3)	90.00	90.00
β [°]	64.02(3)	103.57(3)	105.947(10)
γ [°]	62.13(3)	90.00	90.00
V [Å^3]	3621.1(12)	13509(5)	12011.6(14)
Z	2	4	4
ρ_{calcd} [g cm^{-3}]	1.460	1.520	1.574
μ [mm^{-1}]	1.236	2.706	1.243
$F(000)$	1666	6232	5928
crystal size [mm^3]	$0.22\times0.10\times0.08$	$0.48\times0.13\times0.07$	$0.35\times0.24\times0.13$
θ_{max}	24.35	22.28	28.28
reflns collected	25748	71906	86663
independent reflns	10776 (0.175)	16962 (0.173)	14899 (0.062)
parameters	850	1706	750
GOF on F^2	0.676	0.813	1.055
R_1 [$I>2\sigma(I)$]	0.0594	0.0695	0.0650
wR_2 (all data)	0.1264	0.1277	0.2117
larg. diff. peak/hole [e Å^{-3}]	0.418/−0.461	1.059/−0.786	2.223/−1.476

Interpretation of the magnetic data: Magnetic data have been interpreted by a numerical solution of the Heisenberg–Dirac–van Vleck exchange Hamiltonian, written in the basis of the $N=2^n$ wavefunctions for n interacting $s=1/2$ spin momenta. The matrix of the Hamiltonian has been constructed using Dirac's permutation operator (see Supporting Information) and represented as a sum of matrices times exchange constants for each independent exchange pathway. Intraatomic exchange has been introduced in terms of an arbitrarily large but fixed value of the intraatomic exchange integral ($J=5000$ cm^{-1}). This makes it possible to project a high-spin ground state for Cr^{3+}. A nonlinear optimization procedure has been adopted, which yields exchange coupling constants from the experimental magnetic susceptibility data. The algorithm has been implemented to make it possible also to obtain magnetization values and to fit them to experimental data for the field dependence of the magnetization. A series of programs in Matlab 6.1 have been written; they can be obtained from the authors on request.

Materials: $K_3[Cr(CN)_6]$, $K_3[Fe(CN)_6]$, and $K_3[Co(CN)_6]$ were purchased from Aldrich and used without further purification; $[Cu_3(L)](NO_3)_3(ClO_4)_3\cdot2H_2O$ and $[\{Cu_3(L)\}_2[\{Fe_2(CN)_{11}\}](CN)(NO_3)_4\cdot34H_2O$ were obtained as described previously,[35] and $K_3[Mn(CN)_6]$,[49] $K_4[Mo(CN)_8]\cdot2H_2O$,[50] $K_4[W(CN)_8]\cdot2H_2O$,[51] $K_3[Mo(CN)_8]\cdot H_2O$,[52,53] $K_3[W(CN)_8]\cdot H_2O$,[53] $[(Ph_3P)_2N]_3[Fe(CN)_6]\cdot2H_2O$,[47] and $[(Ph_3P)_2N]_3[Mn(CN)_6]\cdot0.5H_2O$[54] were prepared as described in the literature.

Syntheses: *Caution!* Perchlorate salts of metal complexes are potentially explosive. Although we did not experience any problem, such complexes should be handled very carefully.

$[\{Cu_3(L)\}\{M(CN)_6\}_2]\cdot 17H_2O$ (Cu_6Cr_4, Cu_6Fe_4, and Cu_6Co_4): $K_3[Cr(CN)_6]$ (0.038 g, 0.116 mmol), $K_3[Fe(CN)_6]$ (0.040 g, 0.116 mmol), or $K_3[Co(CN)_6]$ (0.039 g, 0.116 mmol) was dissolved in aqueous $NaNO_3$ (1 mol L^{-1}, 25 mL) and was added slowly to a hot solution (~90 °C) of $[Cu_3(L)](NO_3)_3(ClO_4)_3\cdot 2H_2O$ (0.090 g, 0.065 mmol) in aqueous $NaNO_3$ (1 mol L^{-1}, 50 mL). The cylindrical vessel (30 cm × 4 cm) containing the clear reaction mixture was placed in an open-ended Dewar flask filled with boiling water for slow cooling. After a day, the precipitated product was filtrated off, washed with water, and dried in air. For every compound the yield was about the same: 0.078 g, 0.049 mmol, 83 %. **Cu_6Cr_4**: $C_{42}H_{100}N_{30}O_{17}Cu_3Cr_2$ (1592.07): calcd C 31.69, H 6.33, N 26.39; found C 31.98, H 5.89, N 26.12; **Cu_6Fe_4**: $C_{42}H_{100}N_{30}O_{17}Cu_3Fe_2$ (1599.76): calcd C 31.53, H 6.30, N 26.27; found C 31.82, H 6.28, N 26.49. **Cu_6Co_4**: $C_{42}H_{100}N_{30}O_{17}Cu_3Co_2$ (1605.94): calcd C 31.41, H 6.28, N 26.17; found C 31.79, H 5.99, N 26.61.

$[\{Cu_3(L)\}\{M(CN)_6\}_2]\cdot 17H_2O$ (Cu_6Cr_4[a], Cu_6Fe_4[a], and Cu_6Mn_4[a]): The solid $K_3[Cr(CN)_6]$ (0.017 g, 0.052 mmol), $K_3[Fe(CN)_6]$ (0.018 g, 0.052 mmol), or $K_3[Mn(CN)_6]$ (0.017 g, 0.052 mmol) was added in one portion to the ice-cold solution of $[Cu_3(L)](NO_3)_3(ClO_4)_3\cdot 2H_2O$ (0.040 g, 0.029 mmol) in water (20 mL). The reaction mixture was stirred for 2 h at 0 °C. The precipitated product was centrifuged, washed four times with water by centrifugation, and dried in vacuum. **Cu_6Cr_4**[a]: yield: 0.033 g, 0.021 mmol, 80 %; $C_{42}H_{100}N_{30}O_{17}Cu_3Cr_2$ (1592.07): calcd C 31.69, H 6.33, N 26.39; found C 31.84, H 6.33, N 26.12. **Cu_6Fe_4**[a]: yield: 0.037 g, 0.023 mmol, 89 %; $C_{42}H_{100}N_{30}O_{17}Cu_3Fe_2$ (1599.76): calcd C 31.53, H 6.30, N 26.27; found C 31.98, H 6.27, N 26.71. **Cu_6Mn_4**[a]: yield: 0.030 g, 0.019 mmol, 72 %; $C_{42}H_{100}N_{30}O_{17}Cu_3Mn_2$ (1597.95): calcd C 31.57, H 6.31, N 26.30; found C 31.28, H 6.03, N 26.12.

$[\{Cu_3(L)\}\{M(CN)_8\}](NO_3)_2\cdot 10H_2O$ (Cu_6Mo_2 and Cu_6W_2): $K_4[Mo(CN)_8]\cdot 2H_2O$ (0.021 g, 0.043 mmol) or $K_4[W(CN)_8]\cdot 2H_2O$ (0.025 g, 0.043 mmol) was dissolved in aqueous $NaNO_3$ (1 mol L^{-1}, 80 mL) and was added slowly to a boiling solution of $[Cu_3(L)](NO_3)_3(ClO_4)_3\cdot 2H_2O$ (0.030 g, 0.216 mmol) in aqueous $NaNO_3$ (1 mol L^{-1}, 170 mL). The vessel containing the clear reaction mixture was placed in an open-ended Dewar filled with boiling water for slow cooling. After one day the precipitated product was removed by filtration (only needlelike crystals could be seen under the microscope, so the product was free from **Cu_6Mo** or **Cu_6W** respectively), washed carefully with a small amount of cold water, and dried in air. **Cu_6Mo_2**: yield: 0.045 g, 0.031 mmol, 71 %; $C_{38}H_{86}N_{28}O_{16}Cu_3Mo$ (1477.85): calcd C 30.88, H 5.87, N 26.54; found C 30.81, H 5.85, N 25.97. **Cu_6W_2**: yield: 0.048 g, 0.031 mmol, 71 %; $C_{38}H_{86}N_{28}O_{16}Cu_3W$ (1565.75): calcd C 29.15, H 5.54, N 25.05; found C 29.54, H 5.24, N 24.39. The excess of $[Cu_3(L)]^{6+}$ was recovered from diluted filtrate by sorption on an SP Sephadex-C25 column.

Acknowledgments

Financial support by the German Science Foundation (DFG) is gratefully acknowledged.

[1] O. Kahn, *Molecular Magnetism*, Wiley, New York, **1993**.
[2] J. S. Miller, M. Drillon, *Magnetism: Molecules to Materials II: Molecule-Based Materials*, Wiley-VCH, Weinheim, **2001**.
[3] M. Verdaguer, *Polyhedron* **2001**, *20*, 1115.
[4] J. S. Miller, *Inorg. Chem.* **2000**, *39*, 4392.
[5] J. S. Miller, *MRS Bull.* **2000**, *25*, 60.
[6] T. Glaser, *Inorg. Chem.* **2004**, *43*, 5192.
[7] M. Verdaguer, A. Bleuzen, V. Marvaud, J. Vaissermann, M. Seuleiman, C. Desplanches, A. Scuiller, C. Train, R. Garde, G. Gelly, C. Lomenech, I. Rosenman, P. Veillet, C. Cartier, F. Villain, *Coord. Chem. Rev.* **1999**, *190–192*, 1023.
[8] K. R. Dunbar, R. A. Heintz, *Prog. Inorg. Chem.* **1997**, *45*, 283.
[9] M. Ohba, H. Okawa, *Coord. Chem. Rev.* **2000**, *198*, 313.
[10] W. E. Buschmann, J. L. Manson, J. S. Miller, *Inorg. Chem.* **2001**, *40*, 1926.
[11] W. E. Buschmann, J. S. Miller, *Inorg. Chem.* **2000**, *39*, 2411.
[12] G. Rombaut, M. Verelst, S. Golhen, L. Ouahab, C. Mathoniere, O. Kahn, *Inorg. Chem.* **2001**, *40*, 1151.
[13] J. M. Herrera, V. Marvaud, M. Verdaguer, J. Marrot, M. Kalisz, C. Mathoniere, *Angew. Chem.* **2004**, *116*, 5584; *Angew. Chem. Int. Ed.* **2004**, *43*, 5468.
[14] S. Tanase, F. Tuna, P. Guionneau, T. Maris, G. Rombaut, C. Mathoniere, M. Andruh, O. Kahn, J.-P. Sutter, *Inorg. Chem.* **2003**, *42*, 1625.
[15] M. Pilkington, S. Decurtins, in *Comprehensive Coordination Chemistry II, Vol. 7* (Eds.: J. A. McCleverty, T. J. Meyer), Elsevier, Oxford, **2004**, p. 177.
[16] P. V. Bernhardt, B. P. Macpherson, M. Martinez, *Inorg. Chem.* **2000**, *39*, 5203.
[17] V. Marvaud, C. Decroix, A. Scuiller, F. Tuyeras, C. Guyard-Duhayon, J. Vaissermann, J. Marrot, F. Gonnet, M. Verdaguer, *Chem. Eur. J.* **2003**, *9*, 1692.
[18] V. Marvaud, C. Decroix, A. Scuiller, C. Guyard-Duhayon, J. Vaissermann, F. Gonnet, M. Verdaguer, *Chem. Eur. J.* **2003**, *9*, 1677.
[19] H. J. Choi, J. J. Sokol, J. R. Long, *Inorg. Chem.* **2004**, *43*, 1606.
[20] E. Colacio, M. Ghazi, H. Stoeckli-Evans, F. Lloret, J. M. Moreno, C. Perez, *Inorg. Chem.* **2001**, *40*, 4876.
[21] M. Ohba, H. Okawa, N. Fukita, Y. Hashimoto, *J. Am. Chem. Soc.* **1997**, *119*, 1011.
[22] M. Ohba, N. Usuki, N. Fukita, H. Okawa, *Inorg. Chem.* **1998**, *37*, 3349.
[23] J. L. Heinrich, P. A. Berseth, J. R. Long, *Chem. Commun.* **1998**, 1231.
[24] J. J. Sokol, M. P. Shores, J. R. Long, *Angew. Chem. Int. Ed.* **2001**, *40*, 236.
[25] M. P. Shores, P. A. Berseth, J. R. Long, V. Marvaud, R. Garde, M. Verdaguer, *Inorg. Synth.* **2004**, *34*, 149.
[26] N. Usuki, M. Yamada, M. Ohba, H. Okawa, *J. Solid State Chem.* **2001**, *159*, 328.
[27] N. F. Curtis, in *Comprehensive Coordination Chemistry II, Vol. 1* (Eds.: J. A. McCleverty, T. J. Meyer), Elsevier, Oxford, **2004**, p. 447.
[28] H.-Z. Kou, B. C. Zhou, S. Gao, D.-Z. Liao, R.-J. Wang, *Inorg. Chem.* **2003**, *42*, 5604.
[29] H. Xiang, S. Gao, T.-B. Lu, R. L. Luck, Z.-W. Mao, X.-M. Chen, L.-N. Ji, *New J. Chem.* **2001**, *25*, 875.
[30] T. Lu, H. Xiang, C. Su, P. Cheng, Z. Mao, L. Ji, *New J. Chem.* **2001**, *25*, 216.
[31] E. Colacio, J.-M. Dominguez-Vera, M. Ghazi, R. Kivekas, F. Lloret, J.-M. Moreno, H. Stoeckli-Evans, *Mol. Cryst. Liq. Cryst. Sci. Technol. Sect. A* **1999**, *335*, 995.
[32] E. Colacio, J. M. Dominguez-Vera, M. Ghazi, J. M. Moreno, R. Kivekas, F. Lloret, H. Stoeckli-Evans, *Chem. Commun.* **1999**, 987.
[33] S. Ferlay, T. Mallah, J. Vaissermann, F. Bartolome, P. Veillet, M. Verdaguer, *Chem. Commun.* **1996**, 2481.
[34] H.-Z. Kou, Y.-B. Jiang, B. C. Zhou, R.-J. Wang, *Inorg. Chem.* **2004**, *43*, 3271.
[35] P. Comba, Y. D. Lampeka, A. Y. Nazarenko, A. I. Prikhod'ko, H. Pritzkow, *Eur. J. Inorg. Chem.* **2002**, 1464.
[36] M. K. Saha, F. Lloret, I. Bernal, *Inorg. Chem.* **2004**, *43*, 1969.
[37] K. Nakamoto, *Infrared and Raman Spectra of Inorganic and Coordination Compounds*, 4th ed., Wiley, New York, **1986**.
[38] R. Podgajny, T. Korzeniak, K. Stadnicka, Y. Dromzee, N. W. Alcock, W. Errington, K. Kruczaa, M. Baanda, T. J. Kemp, M. Verdaguer, B. Sieklucka, *Dalton Trans.* **2003**, 3458.
[39] P. Comba, P. Jurisic, Y. D. Lampeka, A. Peters, A. I. Prikhod'ko, H. Pritzkow, *Inorg. Chim. Acta* **2001**, *324*, 99.
[40] A. B. P. Lever, *Inorganic Electronic Spectroscopy*, 2nd ed., Elsevier Science, Amsterdam, **1984**.
[41] B. Bosnich, C. K. Poon, M. L. Tobe, *Inorg. Chem.* **1965**, *4*, 1102.

[42] J. C. A. Boeyens, S. M. Dobson, in *Stereochemical and Stereophysical Behavior of Macrocycles* (Ed.: I. Bernal), Elsevier, Amsterdam, **1987**, p. 1.
[43] A. G. Orpen, L. Bramner, F. H. Allen, O. Kennard, D. G. Watson, R. Taylor, *J. Chem. Soc. Dalton Trans.* **1989**, 1.
[44] P. V. Bernhardt, E. J. Hayes, *J. Chem. Soc. Dalton Trans.* **1998**, 3539.
[45] P. Comba, A. I. Prikhod'ko, unpublished results.
[46] The structure of the manganese complex and its magnetic susceptibility data have been reported previously;[54] we have repeated the measurements in order to eliminate some inconsistencies with water molecules of crystallization.
[47] D. Cauzzi, G. Mori, G. Predieri, A. Tiripicchio, F. Cavatorta, *Inorg. Chim. Acta* **1993**, *204*, 181.
[48] L. Catala, C. Mathoniere, A. Gloter, O. Stephan, T. Gacoin, J.-P. Boilot, T. Mallah, *Chem. Commun.* **2005**, 746.
[49] J. A. Lower, W. C. Fernelius, *Inorg. Synth.* **1946**, *2*, 213.
[50] J. G. Leipoldt, L. D. C. Bok, P. J. Cilliers, *Z. Anorg. Allg. Chem.* **1974**, *409*, 343.
[51] J. G. Leipoldt, L. D. C. Bok, P. J. Cilliers, *Z. Anorg. Allg. Chem.* **1974**, *407*, 350.
[52] B. J. Corden, J. A. Cunningham, R. Eisenberg, *Inorg. Chem.* **1970**, *9*, 356.
[53] H. Baadsgaard, W. D. Treadwell, *Helv. Chim. Acta* **1955**, *38*, 1669.
[54] W. E. Buschmann, L. Liable-Sands, A. L. Rheingold, J. S. Miller, *Inorg. Chim. Acta* **1999**, *284*, 175.

Received: March 31, 2005
Revised: July 29, 2005
Published online: October 13, 2005

